Proceedings of AERO22: 56th 3AF International Conference,
28-30 March 2022, Toulouse, France
https://www.3af-aerodynamics.com/

Towards the Design and Optimisation of Future Compact Aero-Engines: Intake/Fancowl Trade-off Investigation

Fernando Tejero[a,*], David G MacManus[a], Jesus Matesanz-Garcia[a], Avery Swarthout[a], Christopher Sheaf[b]

[a] *Centre for Propulsion Engineering, School of Aerospace, Transport and Manufacturing, Cranfield University, Bedfordshire, United Kingdom, MK43 0AL*
[b] *Rolls-Royce plc., P.O. box 31, Derby, United Kingdom, DE24 8BJ*

Abstract

Relative to in-service aero-engines, the bypass ratio of future civil architectures may increase further. If traditional design rules are applied to these new configurations and the housing components are scaled then it is expected that the overall weight, nacelle drag and the effects of aircraft integration will increase. For this reason, the next generation of civil turbofan engines may use compact nacelles to maximise the benefits from the new engine cycles. This paper presents a multi-level design and optimisation process for future civil aero-engines. An initial set of multi-point, multi-objective optimisations for axisymmetric configurations are carried out to identify the trade-off between intake and fancowl bulk parameters of highlight radius and nacelle length on nacelle drag. Having identified the likely optimal part of the design space, a set of computationally expensive optimisations for 3D non-axisymmetric configurations are performed. The process includes cruise- and windmilling-type operating conditions to ensure aerodynamic robustness of the downselected configurations. Relative to a conventional aero-engine nacelle, the developed process yielded a compact aero-engine configuration with mid-cruise drag reduction of approximately 1.6% of the nominal standard net thrust.

Publisher unconfirmed. This is the Author Accepted Manuscript issued with: Creative Commons Attribution License (CC:BY:4.0).
TPlease refer to any applicable publisher terms of use.

1. Introduction

It is envisaged that the next generation of turbofan engines will operate at low specific thrust and large bypass ratios to enhance the overall propulsive efficiency [1, 2]. As such, the fan diameter may increase to accommodate the specifications of the new cycles [3, 4]. If traditional design rules are applied and the housing components are scaled to accommodate the larger engines, the nacelle wetted area and weight penalties might counterbalance the expected benefits from these new architectures [5, 6]. Therefore, future civil aero-engines may require compact nacelles [7].

The expected trend is that intakes will have a reduced non-dimensional highlight radius (r_{hi}/r_{fan}) and length (L_{int}/r_{fan}), and it is likely that the fancowl length (L_{nac}/r_{hi}) and trailing edge radius (r_{te}/r_{hi}) will also be reduced (Figure 1). Although non-compact intakes with large r_{hi}/r_{fan} values can meet the aerodynamic requirements for the intake range of operability, they can result in an increase in nacelle drag [8]. On the other hand, short fancowls with low L_{nac}/r_{hi} might lead to unfeasible intake configurations. For this new nacelle design challenge there is very limited information in the open literature and, as such, trade-off studies to quantify intake/fancowl compactness on the nacelle drag are required.

Albert and Bestle [9] carried out a combined intake/fancowl optimisation for a 2D axisymmetric configuration. The optimisation process considered cruise (M = 0.78) and quasi-static (M = 0.05) conditions, and for both operating conditions the peak Mach number along the nacelle was reduced. Three different

*Corresponding author.
E-mail address: f.tejero@cranfield.ac.uk

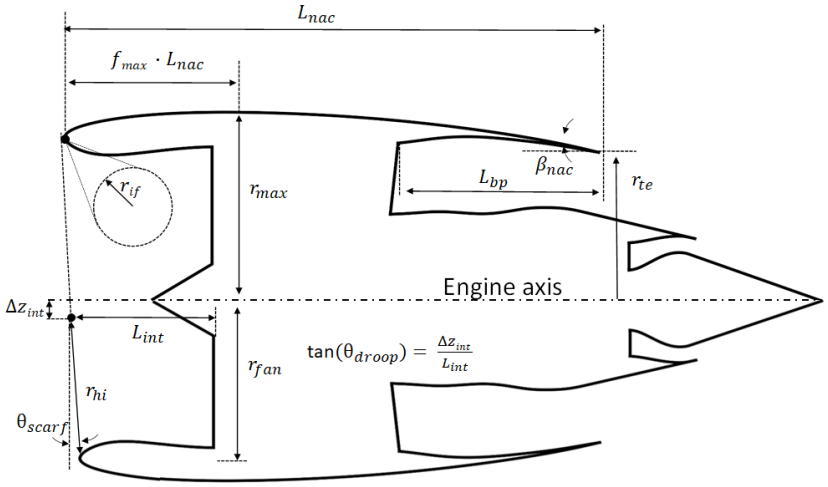


Figure 1: Design variables used to define the aero-engine nacelle

parametrisations for the aero-engine were tested: Superellipse-Polynomial (SP) [10], Class-Shape-Transformation (CST) [11] and B-spline [12]. It was demonstrated that the CST parametrisation provided the best performing set of Pareto optimal solutions. Relative to a reference geometry, the CST approach achieved a reduction of peak Mach number of 14% and 29% for cruise and quasi-static conditions, respectively. The study focused in a single nacelle architecture with fixed r_{hi}/r_{fan} and L_{nac}/r_{hi} and did not extract the nacelle drag. As such, no trade-off between the intake and fancowl bulk dimensions were derived. Toubin *et al.* [13] performed the optimization of a 3D aero-engine nacelle with the MOEA/D evolutionary algorithm [14]. The process considered two operating conditions: cruise (M= 0.82) and crosswind. The study was based on a long nacelle length with $L_{nac}/r_{hi} = 6.5$, in which the objective functions were the nacelle pressure drag coefficient at cruise and the intake circumferential distortion index (CDI) for crosswind. Relative to a reference nacelle, the design process resulted in a design with a reduction in the nacelle pressure drag and CDI of 0.27% and 3.62%, respectively. The study was performed for a single

overall arrangement with fixed r_{hi}/r_{fan} and L_{nac}/r_{hi} and, therefore, the effect of intake and fancowl sizing on the nacelle drag was not assessed. Peters *et al.* [8] developed an integrated design capability for 3D short inlets and nacelles. The tool was used to design a compact and short intake that maintained the isolated propulsor performance of a baseline long configuration. Relative to the reference geometry, a compact intake design with a reduction in nacelle length of $L_{nac}/r_{hi} \approx 0.55$ was derived. For mid-cruise conditions with M = 0.80, the nacelle drag was reduced by about 16% for the short intake configuration. However, this design was not based on a thrust-drag bookkeeping method and only accounted for the pressure and viscous forces that acted on the external wall of the nacelle.

Other investigations considered the nacelle drag as a function of fancowl bulk parameters, e.g. L_{nac}/r_{hi} and r_{te}/r_{hi} (Figure 1). Whilst these studies are of relevance to initially identify the possible limits of the feasible design space for compact configurations, the effect of intake bulk dimensions, such as r_{hi}/r_{fan} or L_{int}/r_{fan}, were neglected. Tejero *et al.* [15] developed a multi-point, multi-objective optimisation tool for the design of UHBPR aero-engine nacelles. The method was used for a range of nacelle lengths ($2.4<L_{nac}/r_{hi}<3.0$) and trailing edge radii ($0.90<r_{te}/r_{hi}<1.0$). A set of MOOs were carried out and the effect of both parameters on nacelle drag was quantified. The process was coupled with an established industrial thrust drag bookkeeping method to extract the drag [16]. Across the design space for future civil aero-engines, the nacelle drag varied by 40%. For compact architectures with $r_{te}/r_{hi} = 0.9$, it was found that small changes on L_{nac}/r_{hi} have a large impact on mid-cruise drag. Schreiner *et al.* [17] further developed the framework and considered windmilling-type conditions during the design process. The study was also based on 2D axisymmetric configurations and highlighted the larger sensitivity of compact aero-engine na-

celles to off-design requirements with respect to conventional architectures. It was concluded that although the nacelle cruise drag could be reduced by about 15% by shortening the nacelle length from $L_{nac}/r_{hi} = 4.3$ to 3.1, this benefit reduced to about 10% once windmilling consideration were accounted to ensure aerodynamic robustness.

There is very limited information in the open literature about multi-point, multi-objective optimisation of 3D non-axisymmetric configurations due to the associated large computational cost. It has been a common practice to design a set of axisymmetric aero-lines and combine them to generate the 3D non-axisymmetric geometry by including the intake scarf and droop angle requirements [18] (Figure 1). However, for compact civil aero-engines in which the inherent non-linearity of transonic flow aerodynamics will arise with respect to conventional configurations, it might be required to perform 3D non-axisymmetric optimisations at an early stage of the design process. The previous studies for 3D non-axisymmetric architectures are mainly based on optimisation processes driven by low order models. Fang *et al.* [19] carried out a MOO for a 3D non-axisymmetric nacelle with $L_{nac}/r_{hi} \approx 3.5$. The nacelles were defined with Class Shape Transformation (CST) curves and 20 degrees of freedom. The Non-dominated Sorting Genetic Algorithm II (NSGA-II) genetic algorithm [20] was employed for the optimisation in which a surrogate model based on the Kriging interpolation method [21] was used to drive the process. Two different transonic conditions at $M_\infty = 0.80$ with AoA = 0° and 4° were considered. Overall, for the relatively large design space considered with twenty design variables, the initial design space exploration and following generations consisted of only 32 configurations due to the large computational cost associated with the 3D RANS solutions. Relative to a baseline geometry, the method identified an optimal nacelle with 4% drag reduction at AoA = 4° and similar drag at AoA

$= 0°$. Zhong *et al.* [22] investigated laminar flow for nacelle applications. The study was based on RANS with the transition SST $\gamma - Re_\theta$ model and used a Kriging interpolation surrogate model to drive the design process. It was focused on transonic conditions at $M_\infty = 0.78$ in which the 3D non-axisymmetric nacelles were defined with 18 design variables. With respect to a reference geometry, the method provided an aero-engine nacelle with a 7% larger laminar area.

This work extends the previous nacelle design method developed by Tejero *et al.* [23, 18, 24] for the multi-point, multi-objective optimisation of ultra high bypass ratio (UHBPR) aero-engine nacelles. Relative to the previous computational approach, the method has been extended to now also include the capability to evaluate the nacelle drag with separate-jet exhausts for UHBPR architectures. The novelty of this paper is in the development of a multi-level, two-step process for the design of compact aero-engine nacelles. The first step is an initial design space exploration for 2D axisymmetric configurations to identify the feasible design space. A set of independent multi-point, multi-objectives optimisation are carried out for a range of intake and fancowl bulk parameters. This study considers the effect of intake compactness (r_{hi}/r_{fan}) and fancowl length (L_{nac}/r_{hi}) on the nacelle drag. For the second part of the process, the optimal regions of the 2D axisymmetric studies are identified and bespoke 3D non-axisymmetric MOOs are performed. The proposed optimisation method considers not only cruise-type conditions but also off-design windmilling requirements.With respect to previous work for nacelle design, the optimisation method encompasses both regression and classification metrics to ensure that the identified Pareto front configurations are aerodynamically feasible. The method is an enabling technology towards the design of future turbofan aero-engines that aim to minimise the fuel burn.

2. Methodology

The numerical approach uses a parametric representation of the different aero-engine housing components [25] (Figure 1). The nacelle drag is evaluated with numerical simulations and extracted with an industrial thrust-drag bookkeeping method [16]. Different conditions of the flight envelope are considered during the design process through a multi-point, multi-objective optimisation routine driven by the Optimized Multi-Objective Particle Swarm Optimization (OMOPSO) gradient-free algorithm [26]. A detailed description of the different modules were previously elaborated [23, 18, 24] and, as such, only a brief description is provided in this paper.

The intake [25], fancowl [15] and separate-jet exhaust [27] are defined using an intuitive Class-Shape Transformation parametrisation [28, 29]. Each nacelle aero-line is controlled with 7 intuitive parameters: r_{hi}, L_{nac}, r_{te}, r_{if}, f_{max}, r_{max} and β_{nac} (Figure 1). Within the context of this work, a set of independent MOOs are carried out at fixed r_{hi}, L_{nac} and r_{te}. As such, the 2D axisymmetric optimisation have four degrees of freedom. The 3D non-axisymmetric configurations are controlled with 5 aero-lines and the intake scarf and droop angles [24] (Figure 1). For this study the scarf and droop angles are also fixed and, therefore, a total of 20 degrees of freedom are used during the MOO of 3D non-axisymmetric aero-engine nacelles. The computational domain is generated with a multi-block structured mesh [30]. A density-based solver is used to solve the compressible steady Favre-averaged Navier-Stokes equations [31] with a second order spatial discretization and the Green-Gauss node based scheme. The k-ω SST model [32, 33] is applied as turbulence closure and the Sutherland's law is used for the calculation of the viscosity [34]. Pressure farfield boundary conditions are used to model the freestream. The Mach number is imposed together with the static pressure and temperature, which are calculated from

the ISA model [35] and the user-prescribed altitude. All the housing component surfaces, i.e. spinner, intake, fancowl, bypass duct the core duct surfaces, are modelled as no-slip adiabatic walls. The flow conditions at the fan face are defined with a target massflow pressure outlet boundary condition, which is derived from the user-prescribed mass flow capture ratio (MFCR). The flow conditions at the bypass and core duct inlets are modelled as pressure inlets using prescribed total pressure and temperature values. The method is coupled with the OMOPSO algorithm [26, 36]. All the multi-point, multi-objective optimisations start with a design space exploration based on a Latin Hypercube Sampling (LHS) [37, 38]. The process is driven with numerical simulations and the convergence criteria of the MOOs is based on the hypervolume indicator [39]. The optimisations were classified as converged when the changes in the hypervolume reduced to below 1%.

For the 2D axisymmetric and 3D non-axisymmetric computational approaches, a grid sensitivity was carried out. It was based on a representative mid-cruise condition of future civil aero-engines (M = 0.85, MFCR = 0.7, h = 10668m) with a short nacelle of $L_{nac}/r_{hi} = 3.1$. Three different cell sizes were considered in which a reference one was selected and a halved and doubled resolution grid were created. The Grid Convergence Index (GCI) of the reference grid was calculated following Roache's method [40]. For the 2D axisymmetric approach and cell sizes 35k, 70k and 140k, a GCI of about 0.70% was achieved. For the 3D non-axisymmetric method with cell sizes of 0.5M, 1.0M and 2.0M provided a GCI of approximately 2.5%. Similar values of GCI have been previously used in optimisation studies for aero-engine nacelle applications [15, 24]. For both numerical approaches the farfield is located at $80r_{max}$. This selection was based on domain sensitivity studies for 2D and 3D configurations [15, 24] in which four different domain sizes ($40r_{max}$, $60r_{max}$, $80r_{max}$ and $100r_{max}$) were considered.

Across this range the cruise nacelle drag increased monotonically with a 0.10% reduction between the $80r_{max}$ and $100r_{max}$ configurations. As such, the $80r_{max}$ domain size is employed in this investigation.

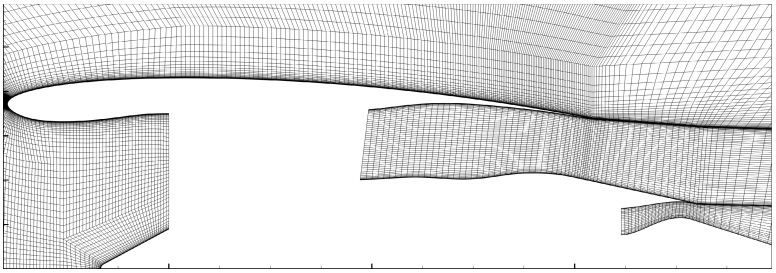


Figure 2: Computational mesh for the 2D axisymmetric numerical model

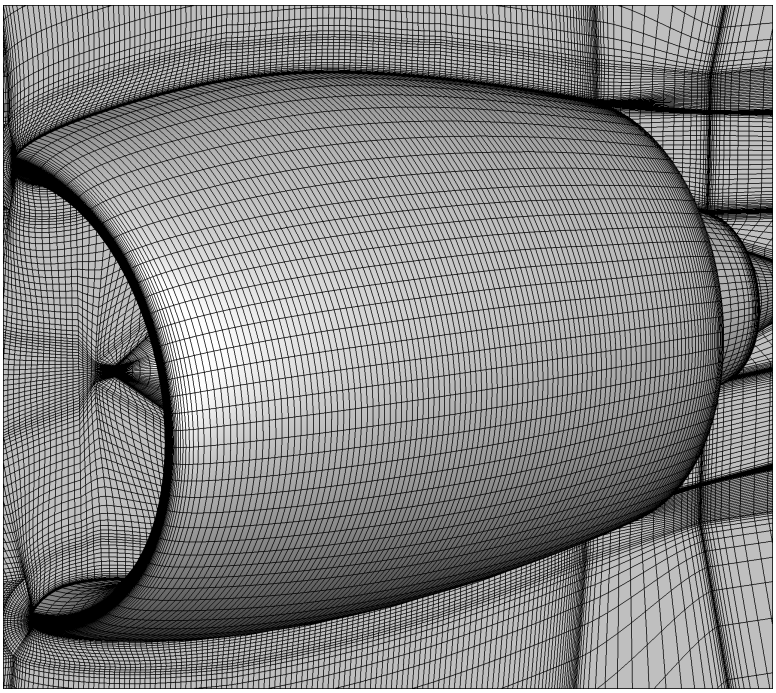


Figure 3: Computational mesh for the 3D numerical model

The numerical methods have been validated with two different nacelle configurations. The 2D axisymmetric numerical approach was compared with a design based on an axisymmetric geometry with a cylindrical centerbody, a

simple circular arc for the forebody, and a straight line for the afterbody [41]. This geometry is referred as Nacelle-1. Conversely, the predictive capability of the 3D numerical method was evaluated against a more modern configuration with no centrebody and a continuously curved geometry from leading to trailing edge [41]. This design is referred as Nacelle-2. For both configurations (Nacelle-1 and Nacelle-2), the nacelle drag for a set of different Mach number was evaluated at a representative cruise MFCR = 0.7. While for the Nacelle-1 the incidence angle was set to 0^o due to the 2D axisymmetric nature of the simulations, the Nacelle-2 3D numerical approach was tested for an incidence angle of 2^o. For a nominal Mach number of M = 0.85, relative to the experimental data the normalised cruise drag is overpredicted by 0.1% and 1.1% for the 2D and 3D numerical approaches, respectively (Figures 4 and 5). The drag rise Mach number (M_{DR}) [15] was predicted within -0.003 and +0.002 for the Nacelle-1 and Nacelle-2 configurations, respectively. To test the effect of reducing the massflow capture ratio in a windmilling scenario, the nacelle drag for a set of MFCR at constant M = 0.85 was performed for the Nacelle-1 design (Figure 6). Within the range of MFCR = 0.5 and 0.4, the nacelle drag was underpredicted by about 4%.

3. Results and analysis

This work develops a multi-level optimisation approach for compact aero-engines nacelles. The process is used to map out the new UHBPR nacelle design challenge and quantify the intake/fancowl trade-off on nacelle drag. For this investigation, two main bulk parameters were considered: r_{hi}/r_{fan} to quantify the intake compactness and L_{nac}/r_{hi} to assess the impact of shortening the fancowl length. The process was initialised with a set of multi-point, multi-objective optimisation for 2D axisymmetric configurations. The baseline geometry is the

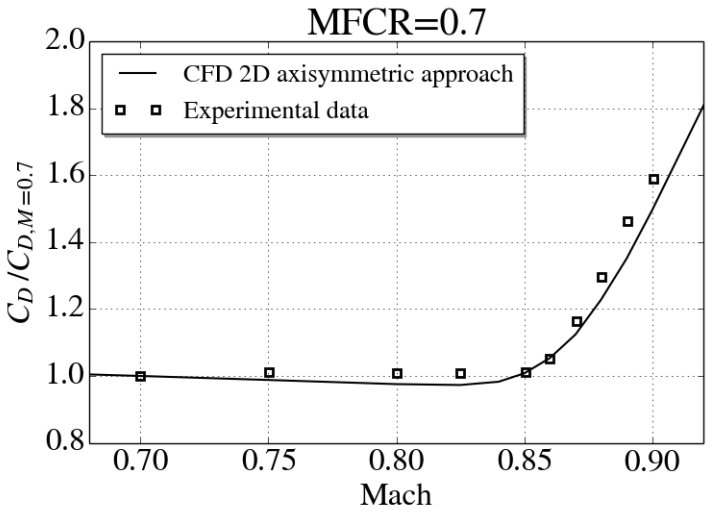


Figure 4: Comparison of nacelle drag as a function of Mach number for the 2D axisymmetric nacelle configuration

optimised design for a conventional configuration with $L_{nac}/r_{hi} = 3.6$ and a nominal r_{hi}/r_{fan}. Overall, 16 independent MOOs were carried out for a full factorial combination of 4 different L_{nac}/r_{hi} and 4 different r_{hi}/r_{fan} values. The nacelle lengths were $L_{nac}/r_{hi} = 2.85$, 3.1, 3.35 and 3.6 and the r_{hi}/r_{fan} values were defined as a reduction relative to the nominal intake compactness with $\Delta r_{hi}/r_{fan} = 0\%, -1.25\%, -2.5\%$ and -3.75%. For the optimal regions of the design space, additional 3D non-axisymmetric MOOs were performed to determine the final designs.

The design and optimisations were undertaken with representative separate-jet exhausts [27]. The aero-engine operates with a bypass ratio above 15 and a nominal standard net thrust (F_N) of about 60kN [27] at mid-cruise conditions. The massflow through the engine was set to have a mass flow capture ratio of MFCR ≈ 0.7 [15] at mid-cruise conditions and $\Delta r_{hi}/r_{fan}$ = -3.75%. As such, the MFCR decreases as the intake is less compact, i.e. larger r_{hi}/r_{fan}.

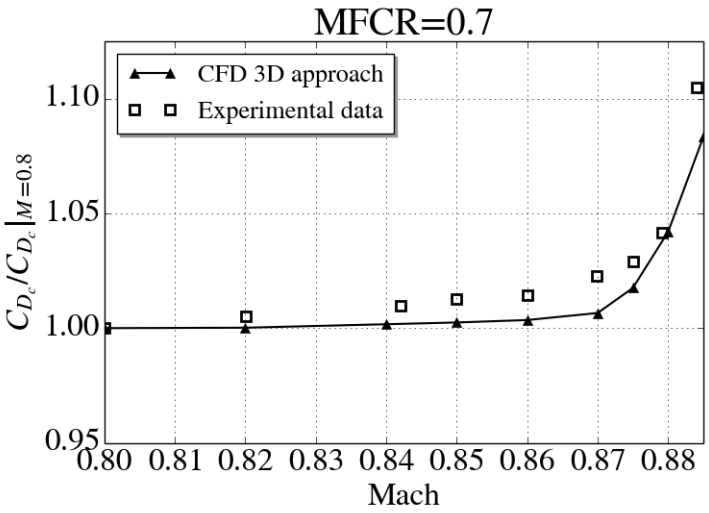


Figure 5: Comparison of nacelle drag as a function of Mach number for the 3D nacelle configuration

3.1. 2D axisymmetric studies

Three flight conditions are used to drive the 2D axisymmetric optimisation routine (Table 1) in the first step of the multi-level design approach. Whilst the mid-cruise drag has a large impact on the overall engine fuel burn, the other two (iM and diversion) are considered to ensure aerodynamic robustness at off-design conditions. They aim to quantify the sensitivity of the nacelle aerodynamics to perturbations on Mach number (iM) and to large changes on the massflow capture ratio (windmilling diversion). The mid-cruise drag (D_{cruise}) and increased Mach number drag (D_{iM}) are considered as regression objective functions (Regr. in Table 1) in which their values are minimised during the MOO process. The windmilling diversion scenario is a combined regression and classification (Regr./Class. in Table 1) objective function. An acceptability threshold on the maximum length of the local boundary layer separation (L_{sep}) was defined for this off-design condition. An acceptability level of L_{sep}/L_{nac} <0.05

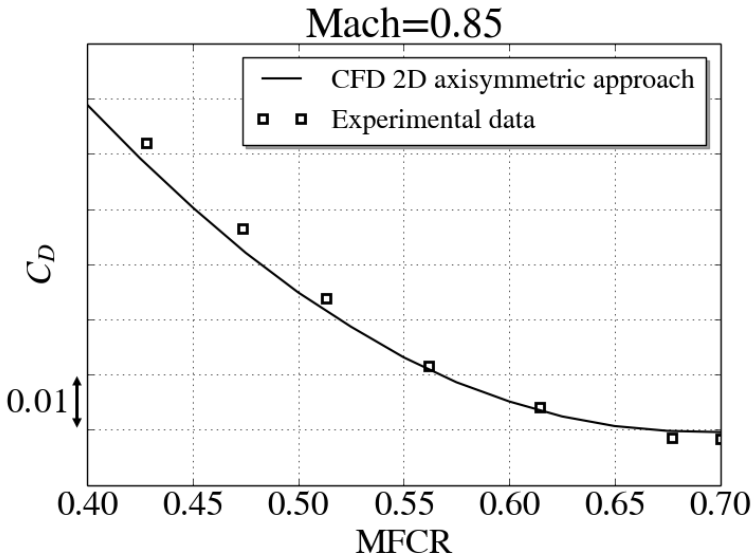


Figure 6: Comparison of nacelle drag as a function of massflow capture ratio for the 2D axisymmetric nacelle configuration

was set for the optimisation. The nacelle diversion drag ($D_{diversion}$) of the designs that fulfill this criteria is minimised and the configuration that exceed it are rejected from the optimisation process. This is to ensure that the MOO is not driven to regions of the design space that are very sensitivity to windmilling off-design conditions. Overall, around 5,500 CFD evaluations are performed in the optimisation routine.

Name	Mach	MFCR	Type
cruise	0.85	0.70	Regr.
iM	0.87	0.70	Regr.
diversion	0.65	< 0.5	Regr./Class.

Table 1: Operating conditions for the 2D axisymmetric MOOs. The MFCR value is for the $\Delta r_{hi}/r_{fan} = -3.75\%$ configuration

An example of the Pareto front from the 2D axisymmetric multi-point, multi-objective optimisation of the reference aero-engine architecture ($L_{nac}/r_{hi} = 3.6$

and $\Delta r_{hi}/r_{fan} = 0\%$) is presented in Figure 7. It presents the results for the non-dominant nacelle designs for a 2D projection in the D_{cruise}-$D_{diversion}$ space and colored with D_{iM}. It highlights the trade-off between nacelle cruise and diversion drag, and demonstrates the importance of including this flight condition in a nacelle optimisation process. Otherwise, the design process would be driven to parts of the design space with low D_{cruise} but that are not aerodynamically feasible due to the large penalties at off-design.

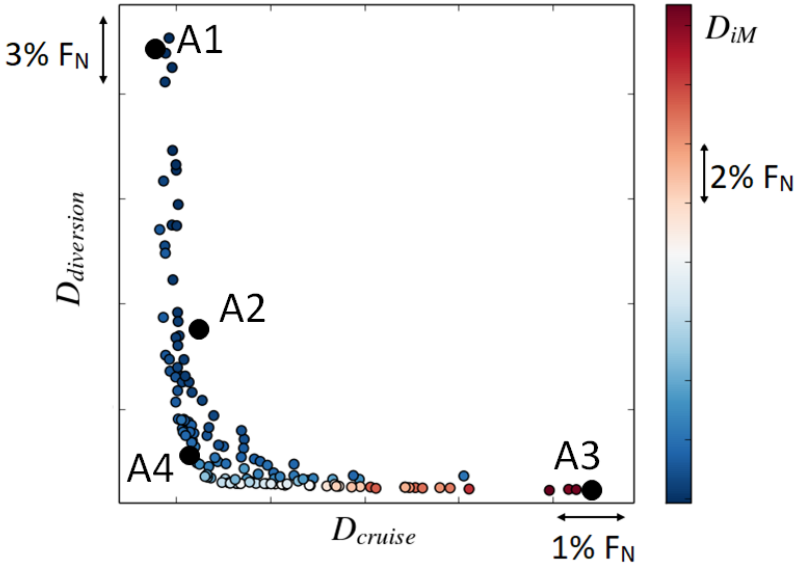


Figure 7: Pareto front for the reference 2D axisymmetric aero-engine nacelle with L_{nac}/r_{hi} = 3.6 and $\Delta r_{hi}/r_{fan} = 0\%$

To provide an initial insight of the transonic flow aerodynamics of aero-engine nacelles four configurations were downselected. They are the configurations with the minimum D_{cruise}, minimum D_{iM}, minimum $D_{diversion}$ and a trade-off design, and are referred as A1, A2, A3 and A4, respectively (Figure 7). Figure 8 presents the isentropic Mach number along the fancowl at mid-cruise conditions for the 4 aero-engine nacelles. There are differences on the initial acceleration around the nacelle lip between the designs. While A1, A2 and A4

have a similar axial location of the peak M_{is} at $X/L_{nac} \approx 0.01$, the design A3 has a change on the flow topology with a continuous acceleration along the nacelle forebody to terminate in a shock wave at $X/L_{nac} \approx 0.41$. Relative to the designs A1 (minimum D_{cruise}) and A4 (trade-off design) that have the same peak M_{is}, the shape A2 (minimum D_{iM}) has a reduction on peak M_{is} of about 0.08. While the design A1 has a smooth flow deceleration along the profile, the designs A2 and A4 have a double shock structure and the design A3 (minimum $D_{diversion}$) has a single strong shock. These changes in the aerodynamics are accompanied by variations on mid-cruise drag. Relative to the minimum cruise drag configuration, A1, the nacelle drag increases by approximately 6.0%, 75.0% and 5.0% for the architectures A2, A3 and A4, respectively.

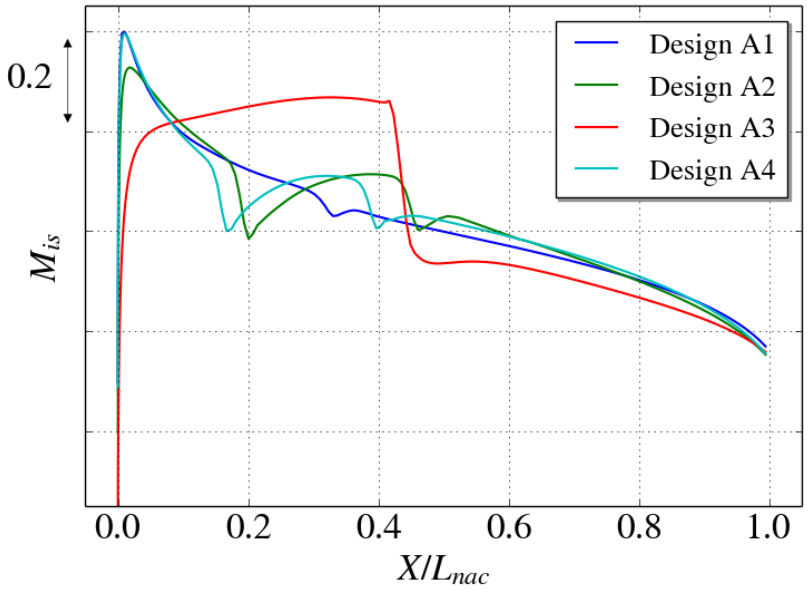


Figure 8: Isentropic Mach number distribution for downselected nacelles of the reference 2D axisymmetric MOO

Having demonstrated the capability of the 2D axisymmetric method for multi-point, multi-objective optimisations, an independent MOO for the full factorial combination of cases with $L_{nac}/r_{hi} = 2.85$, 3.1, 3.35 and 3.6 and

$\Delta r_{hi}/r_{fan} = 0\%, -1.25\%, -2.5\%$ and -3.75%, was performed. For each optimisation a Pareto front was derived from which a nacelle configuration could be downselected. For the reference configuration with $L_{nac}/r_{hi} = 3.6$ and $\Delta r_{hi}/r_{fan} = 0\%$ the downselection criteria was based on the minimum achievable mid-cruise drag with $D_{cruise} < 1.1 \cdot D_{iM}$, in which for the windimilling diversion case the threshold of acceptable local boundary layer separation along the nacelle, i.e. $L_{sep}/L_{nac} < 0.05$, is met. For the rest of configurations, the downselection criteria was based on the minimum achievable D_{cruise}, that have D_{iM} and $D_{diversion}$ lower than the associated drag values of the reference nacelle. Besides, it was also ensured that the configurations met the threshold in flow separation of $L_{sep}/L_{nac} < 0.05$ for the diversion scenario. Figure 9 presents the mid-cruise nacelle drag changes normalised with the nominal standard net thrust across the design space. It highlights the large impact of r_{hi}/r_{fan}. For example, for a fixed $L_{nac}/r_{hi} = 3.1$ which is representative of a compact aero-engine nacelle [23], the normalised drag reduces by 1.6% when the intake highlight is moved inboards from $\Delta r_{hi}/r_{fan} = 0\%$ to $\Delta r_{hi}/r_{fan} = -3.75\%$ (Figure 9). This is caused by the sensitivity of short fancowls to MFCR [15]. Because the massflow through the engine is the same for both configurations ($\Delta r_{hi}/r_{fan} = 0\%$ and $\Delta r_{hi}/r_{fan} = -3.75\%$), the effective MFCR reduces when r_{hi}/r_{fan} increases. On the other hand, for a fixed $\Delta r_{hi}/r_{fan} = -3.75\%$, the normalised drag varies by 0.6% across the range of nacelle lengths considered, in which the minimum value is at $L_{nac}/r_{hi} = 3.1$. Although a further reduction to $L_{nac}/r_{hi} = 2.85$ reduces the wetted area, the design has a stronger shock wave and a concomitant increase in wave drag. This results in a normalised drag penalty of 0.6% with respect to the aerodynamically optimal at $L_{nac}/r_{hi} = 3.1$. Conversely, increasing the L_{nac}/r_{hi} to 3.6 provides a normalised drag penalty of 0.5% (Figure 9).

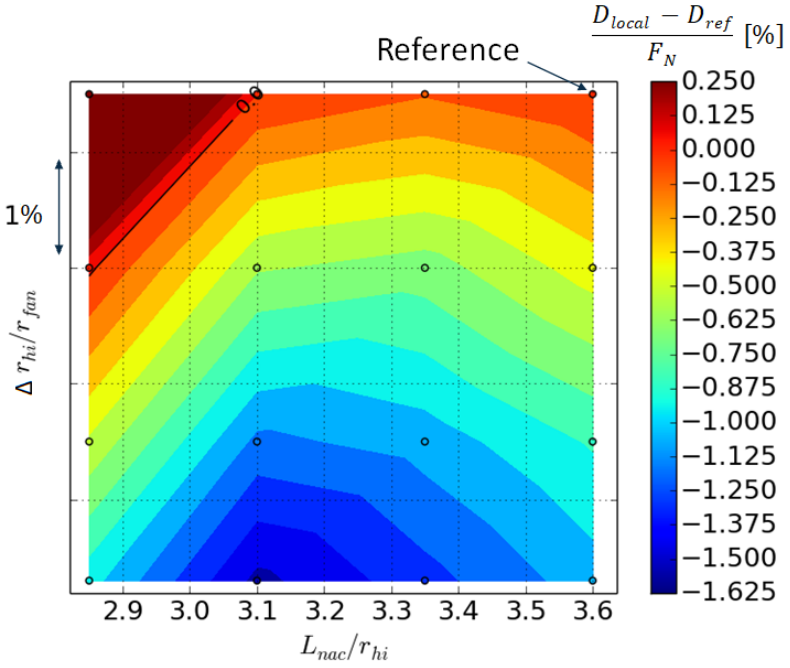


Figure 9: Mid-cruise normalised drag changes with net thrust ($(D_{local}-D_{ref})/F_N$) across the r_{hi}/r_{fan}-L_{nac}/r_{hi} design space considered. D_{ref} refers to the nacelle drag for the reference nacelle with L_{nac}/r_{hi} = 3.6 and $\Delta r_{hi}/r_{fan} = 0\%$

Across the design space, the optimal aero-engine nacelle was at L_{nac}/r_{hi} = 3.1 and $\Delta r_{hi}/r_{fan} = -3.75\%$. Relative to the baseline architecture with L_{nac}/r_{hi} = 3.6 and $\Delta r_{hi}/r_{fan} = 0\%$, the normalised cruise drag is reduced by 1.6%. This initial 2D axisymmetric study has demonstrated the potential benefits of compact nacelle for future civil aero-engines and has quantified the impact of the bulk parameters L_{nac}/r_{hi} and r_{hi}/r_{fan} on nacelle drag (Figure 9).

3.2. 3D non-axisymmetric studies

The first step of the multi-level optimisation process has demonstrated the large impact of intake compactness (r_{hi}/r_{fan}) on nacelle cruise drag (Figure 9). For the two most compact intake configurations considered ($\Delta r_{hi}/r_{fan} = -2.5\%$ and -3.75%), the optimal nacelle length is L_{nac}/r_{hi} = 3.1. As such, an investiga-

tion for 3D non-axisymmetric architectures around this part of the design part has been carried out. Overall, four independent 3D MOOs were performed to understand the effect of r_{hi}/r_{fan} on short nacelles. For a fixed $L_{nac}/r_{hi} = 3.1$, three different intakes were considered: $\Delta r_{hi}/r_{fan} = -2.0\%, -3.0\%$ and -3.75%. A MOO for the reference geometry with $L_{nac}/r_{hi} = 3.6$ and $\Delta r_{hi}/r_{fan} = 0\%$ was conducted to establish a 3D baseline aero-engine nacelle.

The multi-point, multi-objective optimisation process is driven with four different operating conditions (Table 2). The first three ones (cruise, iM and diversion) are similar to the 2D axisymmetric MOOs in which the only difference is that the angle of attack was set to 4.5^o. This is to mimic a similar effective incidence of an installed configuration. The 3D MOOs also include a windmilling end-of-runway (EoR) high angle of attack scenario. The nacelle drag for this flight condition is not minimised during the optimisation but classified based on local boundary layer separation (L_{sep}). As for the windmilling diversion case, the acceptability threshold was defined as L_{sep}/L_{nac} <0.05. This is to ensure that the designs that progress through the generations of the MOO are aerodynamically robust. Overall, around 10,000 CFD evaluations are performed in the optimisation routine.

Name	Mach	MFCR	AoA	Type
cruise	0.85	0.70	4.5	Regr.
Mach	0.87	0.70	4.5	Regr.
diversion	0.65	< 0.5	4.5	Regr./Class.
EoR	0.25	< 0.5	20.0	Class.

Table 2: Operating conditions for the 3D non-axisymmetric MOOs. The MFCR value is for the $\Delta r_{hi}/r_{fan} = -3.75\%$ configuration

Having computed the four independent 3D MOOs, a set of Pareto optimal designs were determined. To aid with the comparison of the optimal nacelle configurations for the four 3D optimisations, a comparison of the Pareto fronts

only on the D_{cruise}-$D_{diversion}$ space is shown in Figure 10. For the three configurations with $L_{nac}/r_{hi} = 3.1$ there are designs that reduce both the mid-cruise drag and diversion with respect to the optimal designs from the reference geometry ($L_{nac}/r_{hi} = 3.6$ and $\Delta r_{hi}/r_{fan} = 0\%$). It highlights the benefits of compact aero-engine nacelles with respect to the current in-service architecture.

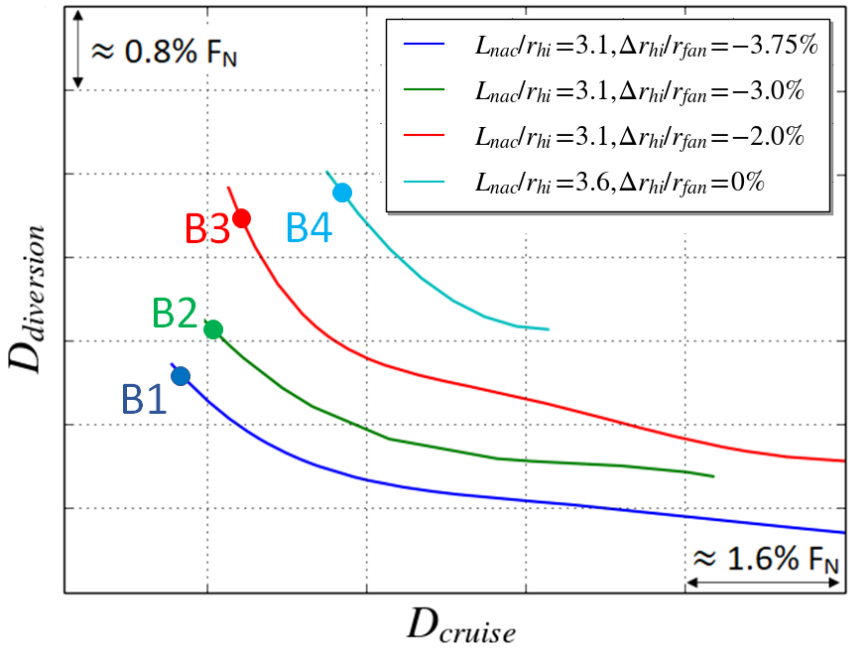


Figure 10: Projection into the D_{cruise}-$D_{diversion}$ space of the Pareto fronts for the 3D configurations

A trade-off nacelle was downselected from each of the MOOs and further investigated. They are referred to B1, B2, B3 and B4 for the $\Delta r_{hi}/r_{fan} = -3.75\%, -3.0\%$ and -2.0% at fixed $L_{nac}/r_{hi} = 3.1$ and $\Delta r_{hi}/r_{fan} = 0\%$ at $L_{nac}/r_{hi} = 3.6$, respectively (Figure 10). For the B4 design, the downselection criteria was based on the minimum achievable mid-cruise drag that satisfies $D_{cruise} < 1.1 \cdot D_{iM}$ and the threshold of acceptable local boundary layer separation along the nacelle of $L_{sep}/L_{nac} < 0.05$ is met for the windmilling diversion and windmilling end-of-runway high angle of attack scenario (Table 2). For the

other configurations, i.e. B1, B2 and B3, the downselection criteria was based on the minimum achievable mid-cruise drag in which the drag for an increased Mach number (D_{iM}) and windmilling diversion ($D_{diversion}$) was lower than for the B4 design, whilst the flow separation threshold of $L_{sep}/L_{nac} < 0.05$ was also fulfilled for both windmilling conditions. For example, for the most compact nacelle considered in this study, i.e. B1 ($\Delta r_{hi}/r_{fan} = -3.75\%$), the normalised mid-cruise drag with respect to the net thrust can be reduced by up to 1.6% with respect to the B4 design. A similar value was obtained with the 2D axisymmetric MOO studies (Figure 9). The benefit identified for the B1 design reduces to approximately 1.2% and 1.0% when the intake highlight is moved outboard to $\Delta r_{hi}/r_{fan} = -3.0\%, -2.0\%$, respectively (Figure 10). This outcome demonstrates that the intake compactness is a key design variable to achieve low values of nacelle drag for short configurations (L_{nac}/r_{hi}) that are expected in future civil aero-engine nacelles [23]. This study quantifies the impact of intake compactness on nacelle drag. However it is important to note that the feasibility of these configurations to meet the off-design intake requirements should be considered within a complete aero-engine nacelle design process [8]. Nevertheless, this work provides for the first time an initial step in quantifying the nacelle drag as a function of the intake bulk parameter r_{hi}/r_{fan} within the envisaged design space for UHBPR aero-engine nacelles.

To provide a better insight of the flow physics of compact configurations, the isentropic Mach number distribution for the optimal nacelle B1 (L_{nac}/r_{hi} = 3.1 and $\Delta r_{hi}/r_{fan} = -3.75\%$) and the baseline geometry B4 (L_{nac}/r_{hi} = 3.6 and $\Delta r_{hi}/r_{fan} = 0\%$) are presented in Figure 11. Both configurations have a stronger initial acceleration around the nacelle lip at the top-line ($\psi = 0^o$) and the top-control line ($\psi = 45^o$) than for the other lines. The peak M_{is} for the compact geometry (B1) is 0.02 larger with respect to the reference one

(B4). For both housing component styles there is an initial shock wave on the nacelle forebody, which is followed by a re-acceleration and a second weaker shock around the nacelle crest. Both shock structures are found in all cross-sections and the strength mitigates azimuthally from the top-line ($\psi = 0^o$) to the bottom-line ($\psi = 180^o$) (Figure 11). Relative to the B1 design, similar flow physics were found for the compact B2 and B3 geometries.

For the downselected aero-engine nacelles derived from the four 3D MOOs (B1, B2, B3 and B4), the nacelle drag sensitivity to Mach number and MFCR was investigated. This is to quantify the aerodynamic performance across a wide range of operating conditions that might be encountered throughout the flight envelope. For the Mach number variations and relative to the conventional nacelle (B4) with L_{nac}/r_{hi} = 3.6 and $\Delta r_{hi}/r_{fan}$ = 0%, the most compact architecture B1 present benefits for all flight Mach number. Whilst for the cruise Mach number of 0.85, the normalised drag benefit is 1.6%, this reduces to 1.3% and 0.6% at M = 0.87 and 0.88, respectively. For the B2 and B3 designs there are drag benefits with respect to the reference B4 for Mach numbers between M = 0.80 and 0.87 (Figure 12). However both designs (B2 and B3) have a normalised nacelle drag penalty of about 1.5% at M = 0.88 relative to B4. This is due to the greater sensitivity of both compact architectures (B2 and B3) to Mach number caused by operating at lower mid-cruise MFCR than the B1 design. For the massflow capture ratio variations, all the short fancowls have drag benefits at relatively high MFCR with respect to the reference L_{nac}/r_{hi} = 3.6 and $\Delta r_{hi}/r_{fan}$ = 0% configuration (Figure 13). However, the benefits erode for low MFCR values due to the large sensitivity of short fancowl to low massflow capture ratios [17].

4. Conclusions

This paper has presented a multi-level two-step process for the design and optimisation of compact civil aero-engine nacelles. It starts with multi-point, multi-objective optimisations of 2D axisymmetric configurations to initially identify the potential optimal parts of the design space. For selected configurations, bespoke 3D non-axisymmetric optimisations are performed. Different operating points of the flight envelope are considered to ensure aerodynamic robustness. They include flight conditions of the cruise segment as well as off-design windmilling scenarios. The optimisation process is driven with regression and classification objective functions to ensure that the identified configurations are aerodynamically feasible. The developed method has been used for intake/fancowl trade-off studies, in which the effects of intake compactness and fancowl length on the nacelle drag have been quantified. It has been demonstrated the large influence of intake compactness on the nacelle drag characteristics. It is noted that the feasibility of the optimised configurations to meet off-design intake requirements should be considered within a complete aero-engine nacelle design process. However, the developed method establish the first step in quantifying the nacelle drag as part of an intake design procedure for ultra-high bypass ratio architectures. Relative to a more conventional aero-engine nacelle, the developed process has yielded a compact nacelle configuration with approximately a mid-cruise nacelle drag reduction of 1.6% of the nominal standard net thrust.

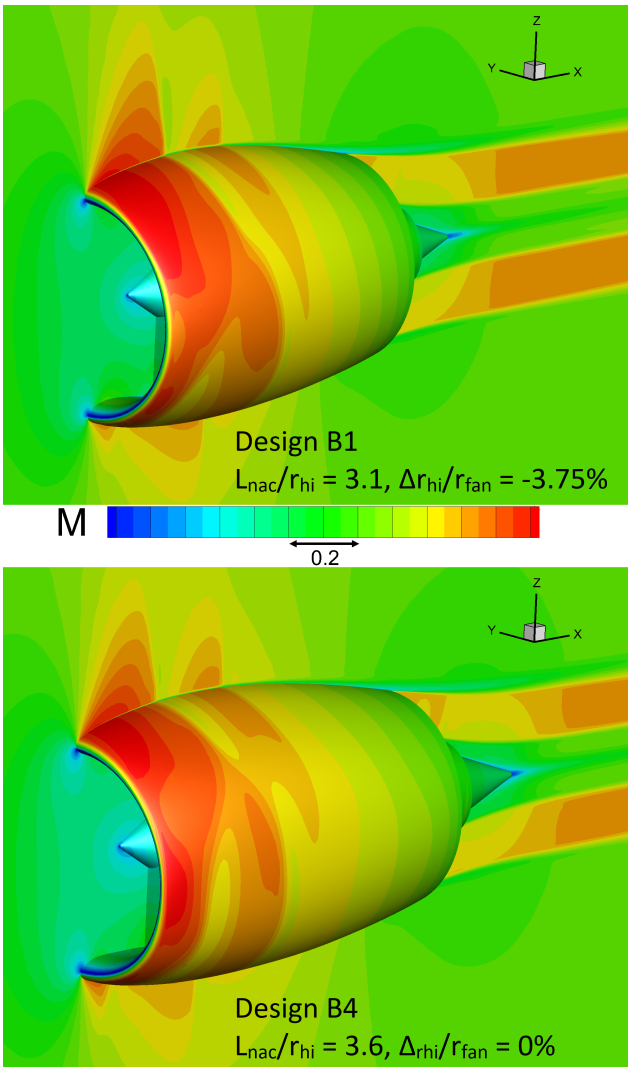


Figure 11: Mach number comparison for the downselected compact design B1 and the baseline architecture B4

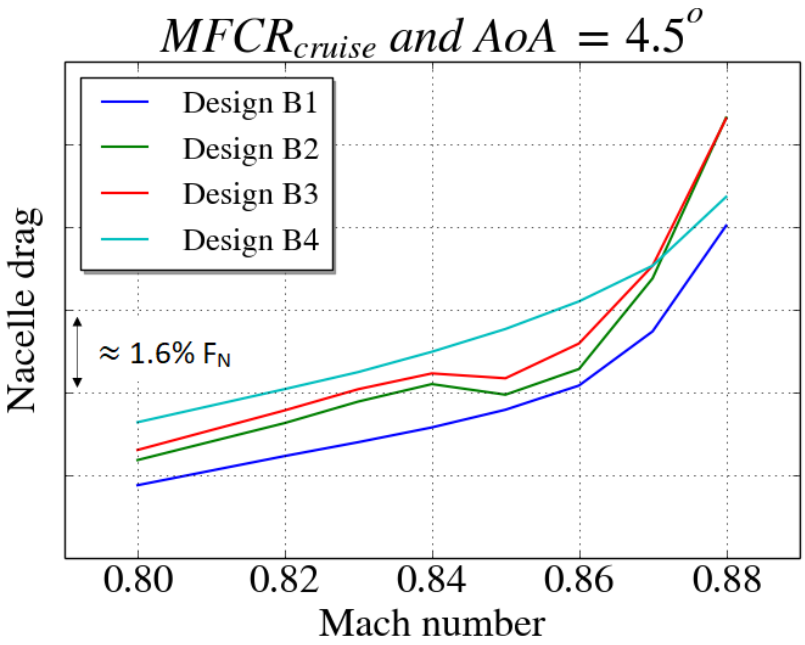


Figure 12: Comparison of nacelle drag as a function of Mach number for the downselected 3D nacelles

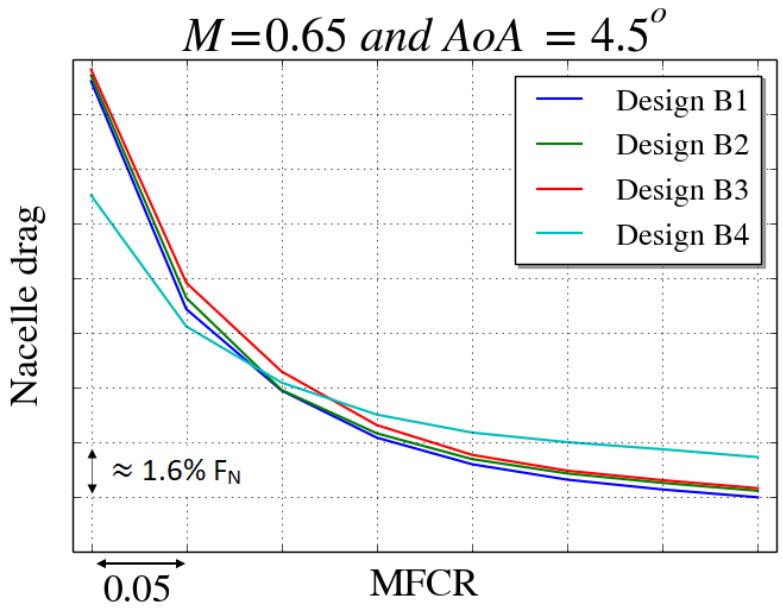


Figure 13: Comparison of nacelle drag as a function of massflow capture ratio for the downselected 3D nacelles

5. Data Statement

Due to commercial confidentiality agreements the supporting data is not available

6. Acknowledgments

This work was partially funded by the INNOVATE UK FANFARE project. It included the tools, methods development and 2D design studies.

This project has received funding from the Clean Sky-2 Joint Undertaking (JU) under grant agreement No-101007598 – ODIN Project. The JU receives support from the European Union's Horizon 2020 research and innovation programme and the Clean Sky 2 JU members other than the Union. This funding covered the 3D design studies.



References

[1] D. Daggett, Ultra-Efficient Engine Technology Systems Integration and Environmental Assessment, Tech. Rep. CR-2002-211754, NASA (2002).

[2] D. Daggett, S. Brown, R. Kawat, Ultra-Efficient Engine Diameter Study, Tech. Rep. CR-2003-212309, NASA (2003).

[3] N. Birch, 2020 Vision: The Prospects for Large Civil Aircraft Propulsion, The Aeronautical Journal 104 (1038) (2000) 347–352.

[4] N. A. Cumpsty, Preparing for the Future: Reducing Gas Turbine Environmental Impact—IGTI Scholar Lecture, Journal of Turbomachinery 132 (2010) 041017.

[5] I. Goulos, J. Otter, F. Tejero, J. H. Rebassa, D. MacManus, Civil Turbofan Propulsion Aerodynamics: Thrust-Drag Accounting and Impact of Engine Installation Position, Aerospace Science and Technology 111 (2021) 106533.

[6] J. Marx, Installation Features of Advances, Very High Bypass Turbofan Propulsion Systems, in: AIAA/AHS/ASEE Aircraft Design, Systems and Operations Conference, AIAA Paper 2015-3778, 2015.

[7] F. Tejero, I. Goulos, D. MacManus, C. Sheaf, Effects of Aircraft Integration on Compact Nacelle Aerodynamics, in: AIAA SciTech 2020 Forum and Exposition, AIAA Paper 2020-2225, 2020.

[8] A. Peters, Z. S. Spakovszky, W. Lord, B. Rose, Ultrashort Nacelles for Low Fan Pressure Ratio Propulsors, Journal of Turbomachinery 137 (2).

[9] M. Albert, D. Bestle, Aerodynamic Design Optimization of Nacelle and Intake, in: Proceedings of ASME Turbo Expo 2013: Turbine Technical Conference and Exposition, no. GT2013-94857, American Society of Mechanical Engineers, 2013.

[10] P. Rosin, G. West, Curve Segmentation and Representation by Superellipses, IEE Proceedings - Vision, Image and Signal Processing 142 (1995) 280 – 288.

[11] B. Kulfan, Recent Extensions and Applications of the 'CST' Universal Parametric Geometry Representation Method, Aeronautical Journal 114 (1153) (2010) 157–176.

[12] I. J. Schoenberg, Spline Functions and the Problem of Graduation, Proceedings of the National Academy of Sciences of the United States of America 52 (4) (1964) 947–950.

[13] H. Toubin, I. S. E. Dim, M. Meheut, Multipoint Aerodynamic High Fidelity Shape Optimization of an Isolated Engine Nacelle, in: AIAA SciTech Forum 52nd Aerospace Sciences Meeting, AIAA Paper Number 014-0903, Virginia Beach, VA, USA, 2014.

[14] Q. Zhang, H. Li, MOEA/D: A Multiobjective Evolutionary Algorithm Based on Decomposition, IEEE Transactions on Evolutionary Computatio 11 (6) (2007) 712–731.

[15] F. Tejero, M. Robinson, D. MacManus, C. Sheaf, Multi-Objective Optimization of Short Nacelles for High Bypass Ratio Engines, Aerospace Science and Technology 91 (2019) 410–421.

[16] Study Group MIDA, Guide to In-Flight Thrust Measurement of Turbojets and Fan Engines, in: Technical Report AGARD-AG-237, Advisory Group for Aerospace Research and Development, 1979.

[17] B. D. J. Schreiner, F. Tejero, D. MacManus, C. Sheaf, Robust aerodynamic design of nacelles for future civil aero-engines, in: Proceedings of ASME Turbo Expo 2020: Turbomachinery Technical Conference and Exposition, GT2020-14470, 2020.

[18] F. Tejero, D. MacManus, C. Sheaf, Impact of Droop and Scarf on the Aerodynamic Performance of Compact Aero-Engine Nacelles, in: AIAA SciTech 2020 Forum and Exposition, AIAA Paper 2020-1522, 2020.

[19] X. Fang, Y. Zhang, S. Li, , H. Chen, Transonic Nacelle Aerodynamic Optimization Based on Hybrid Genetic Algorithm, in: 17th AIAA/ISSMO Mul-

tidisciplinary Analysis and Optimization Conference, AIAA AVIATION Forum, AIAA Paper Number 2016-3833, 2016.

[20] K. Deb, A. Pratap, S. Agarwal, T. Meyarivan, A Fast and Elitist Multiobjective Genetic Algorithm: NSGA-II, IEEE Transactions on Evolutionary Computation 6, (2) (2002) 182 – 197.

[21] T. Simpson, T. M. Mauery, J. J. Korte, F. Mistree, Kriging Models for Global Approximation in Simulation-Based Multidisciplinary Design Optimization, AIAA Journal 39 (12) (2001) 2233–2241.

[22] Y. Zhong, S. Li, A 3D Shape Design and Optimization Method for Natural Laminar Flow Nacelle, in: Proceedings of ASME Turbo Expo 2017: Turbomachinery Technical Conference and Exposition, Paper Number GT2017-64379, Vol. 1, 2017, pp. 825–830.

[23] F. Tejero, D. MacManus, C. Sheaf, Surrogate-Based Aerodynamic Optimisation of Compact Nacelle Aero-Engines, Aerospace Science and Technology 93 (2019) 105207.

[24] F. Tejero, R. Christie, D. MacManus, C. Sheaf, Non-axisymmetric aero-engine nacelle design by surrogate-based methods, Aerospace Science and Technology 117 (2021) 106890.

[25] R. Christie, M. Robinson, F. Tejero, D. MacManus, The Use of Hybrid Intuitive Class Shape Transformation Curves in Aerodynamic Design, Aerospace Science and Technology 95 (2019) 105473.

[26] M. Sierra, C. C.A Coello Coello, Improving PSO-Based Multi-objective Optimization Using Crowding, Mutation and ϵ-Dominance, in: Evolutionary Multi-Criterion Optimization, Springer Berlin Heidelberg, 2005, pp. 505–519.

[27] I. Goulos, T. Stankowski, J. Otter, D. MacManus, N. Grech, C. Sheaf, Aerodynamic Design of Separate-Jet Exhausts for Future Civil Aero-Engine, Part 1: Parametric Geometry Definition and CFD Approach, Journal of Engineering for Gas Turbines and Power 138 (8).

[28] R. Christie, A. Heidebrecht, D. G. MacManus, An Automated Approach to Nacelle Parameterisation Using Intuitive Class Shape Transformation Curves, Journal of Engineering for Gas Turbines and Power 139 (6) (2017) 062601–1 – 062601–9.

[29] J. Matesanz-Garcia, R. Christie, F. Tejero, D. MacManus, A. Heidebrecht, An Automated Approach for the Aerodynamic Design of Close-Coupled Propulsion/Airframe Configurations, in: Aerospace Europe Conference 2020, 2020.

[30] Ansys Inc., 275 Technology Drive, Canonsburg, PA 15317, ANSYS ICEM CFD Tutorial Manual.

[31] Ansys Inc., 275 Technology Drive, Canonsburg, PA 15317, ANSYS FLUENT User's Guide.

[32] F. R. Menter, Two-Equation Eddy-Viscosity Turbulence Models for Engineering Applications, AIAA Journal 32 (8) (1994) 1598–1605.

[33] Y. Jang, J. Huh, S. Lee, Y. Park, Comparative Study on the Prediction of Aerodynamic Characteristics of Aircraft with Turbulence Models, International Journal of Aeronautical and Space Sciences 19 (2018) 13–23.

[34] W. Sutherland, The Viscosity of Gases and Molecular Force, Philosophical Magazine 5 (35) (1893) 507–531.

[35] ISO International Standard 2533-1975, Standard Atmosphere First Edition, Tech. rep., ISO, Geneva, Switzerland (1978).

[36] L. Li, J. Bai, T. Guo, X. He, Z. Fu, Aerodynamic Design of the Supersonic Aircraft Wing-Shape and Wing-Twist Optimization, International Journal of Aeronautical and Space Sciences 19 (2018) 340–353.

[37] J. C. Helton, F. J. Davis, Latin Hypercube Sampling and the Propagation of Uncertainty in Analyses of Complex Systems, Engineering and System Safety 81 (2003) 23–69.

[38] K. Wansaseub, S. Sleesongsom, N. Panagant, N. Pholdee, S. Bureerat, Surrogate-Assisted Reliability Optimisation of an Aircraft Wing with Static and Dynamic Aeroelastic Constraints, International Journal of Aeronautical and Space Sciences 21 (2020) 723–732.

[39] A. Auger, J. Bader, D. Brockhoff, E. Zitzler, Hypervolume-Based Multiobjective Optimization: Theoretical Foundations and Practical Implications, Theoretical Computer Science 425 (2012) 75–103.

[40] P. Roache, A Method for Uniform Reporting of Grid Refinement Studies, Journal of Fluids Engineering 116 (3) (1994) 405–413.

[41] M. Robinson, D. MacManus, C. Sheaf, Aspects of Aero-Engine Nacelle Drag, Proceedings of the Institution of Mechanical Engineers, Part G: Journal of Aerospace Engineering 233 (5) (2018) 1667–1682.



https://dspace.org/

Towards the design and optimisation of future compact aero-engines: intake/fancowl trade-off investigation

Tejero, Fernando; MacManus, David G.; Matesanz García, Jesús; Swarthout, Avery E.; Sheaf, Christopher T.

2022-03-30
Association Aeronautique et Astronautique de France (3AF)
https://www.3af-aerodynamics.com/
Tejero F, MacManus D, Matesanz-Garcia J, et al., (2022) Towards the design and optimisation of future compact aero-engines: intake/fancowl trade-off investigation. In: AERO2022: 56th 3AF International Conference, 28-30 March 2022, Toulouse, France

Downloaded from a DSpace repository. https://dspace.org/